Analysis of optical axis variations in monolithic nonplanar ring laser

Tao Feng (冯 滔)[1,2*], Zhaoyang Jiao (焦兆阳)[1,2], Qiong Zhou (周 琼)[1,2], Mingying Sun (孙明营)[1,2], and Jianqiang Zhu (朱健强)[1]**

[1] *Shanghai Institute of Optics and Fine Mechanics, Chinese Academy of Sciences, Shanghai 201800, China*

[2] *University of Chinese Academy of Sciences, Beijing 100049, China*

[*] *Corresponding author: fengtao1987@siom.ac.cn;* [**] *corresponding author: jqzhu@siom.ac.cn*

Received October 8, 2013; accepted November 19, 2013; posted online December 25, 2013

A mathematical model of the mirror misalignment of a four-equal-sided nonplanar ring cavity is established in this letter. The variations in the optical axis are discussed through an augmented 6 × 6 ray matrix formulation. Numerical analysis shows that the self-consistence of the optical axis can always be obtained because of the thermal effects in any case of mirror misalignment. For a fabricated design, optical axis variations always appear. The influence of thermal effects (i.e., pump power) on optical axis variations are studied. The tilt of the optical axis remains constant, whereas its decentration varies with pump power. Further analysis shows that the actual closing point of the optical axis moves close to the ideal point as the pump power increases. The theoretical analysis proposed is proven and validated by the experimental results.

OCIS codes: 140.3410, 140.3560, 140.3570.
doi: 10.3788/COL201412.011402.

Nonplanar ring oscillators (NPROs) were first introduced in 1985 by Kane *et al.* in an end-pumped configuration with argon-ion laser[1]. Since then, NPROs pumped by laser diodes have been widely investigated because of their excellent properties, such as compactness, reliability, high output power, and good beam quality[2,3]. In active mediums doped with different ions, the energy levels are different[4], so that the nonplanar monolithic ring lasers can be obtained and operated in various wavelengths[5–8]. Kane *et al.* described the principle of NPROs. Nilsson *et al.*[9] expounded the polarization matching theory of geometrical structure parameters design. Zang *et al.*[10] investigated the tradeoffs between minimizing the magnetic field and finding a reasonable fabrication tolerance in the design of NPROs.

NPRO laser is expected to operate with a stable optical axis in various applications. However, the actual optical axis always deviates from the ideal because of inevitable fabrication errors that are incurred in the manufacturing process of NPRO crystal. These deviations are called optical axis variations, which include optical axis decentration and tilt, as defined in below paragraphs. The optical axis variations caused by the errors in the manufacture of monolithic crystals affect the output beam modes, output power, and even the self-consistence of the optical axis. To analyze optical axis variations and reduce them during the operation of the laser, we establish a mathematical model of the optical axis variations of NPRO by using a ray matrix. The relationship between the optical axis variations and pump power is discussed to offer a theoretical guide to the optimization of NPRO laser.

Figure 1 shows the typical configuration of NPRO. To simplify the analysis, a four-equal-sided nonplanar ring resonator was chosen, as shown in Fig. 2. The optical surfaces that contain points A, B, C, and D in Fig. 1 were transformed into mirrors M_1, M_2, M_3, and M_4, respectively, in Fig. 2, respectively. Because of end-face deformation caused by thermal effects, M_1 is equivalent to a spherical mirror with a radius R, and the others are plane mirrors. The incident and refracted angles are θ and α, respectively. The dihedral angle is β, which can be designed from ∼1° to 90°. Triangles ABC and ADC are symmetrical, so $L_1 = L_4$ and $L_2 = L_3$. The total cavity length L is derived from $L = L_1 + L_2 + L_3 + L_4$, which can be calculated with parameters α, β, AE, and CE.

Optical axis variations, including decentration and tilt, occur because of the errors incurred in the manufacture of

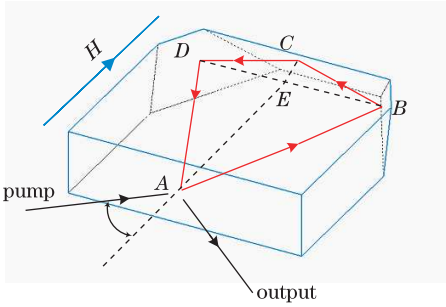

Fig. 1. (Color online) Typical monolithic NPRO.

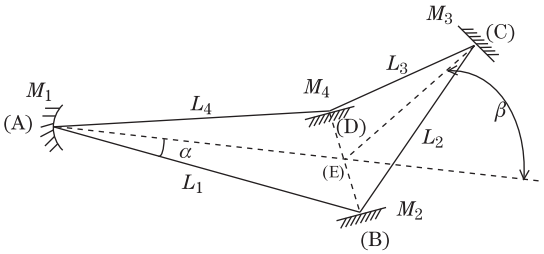

Fig. 2. Four-equal-sided nonplanar ring cavity used in the analysis.

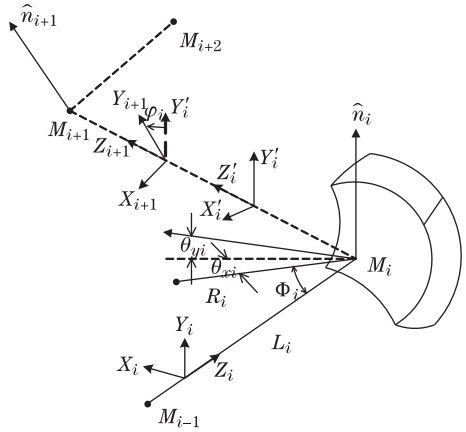

Fig. 3. One single segment of a general resonator[14].

monolithic crystal. To conveniently examine the optical axis variations in the cavity, the manufacturing errors must be regarded as mirror misalignments[11,12] in two orthogonal planes. The augmented 6 × 6 ray matrices are applied[13,14].

An NPRO resonator consists of four segments. Figure 3 shows that each segment contains three element matrices: free-space propagation $T(L_i)$, reflection on the spherical mirror $T(R_i, \phi_i)$, and coordinate rotation $T(\theta_i)$. The matrices $T(L_i)$, $T(R_i, \phi_i)$, and $T(\theta_i)$ may be written as[13−16]

$$T(L_i) = \begin{pmatrix} 1 & L_i & 0 & 0 & 0 & 0 \\ 0 & 1 & 0 & 0 & 0 & 0 \\ 0 & 0 & 1 & 0 & 0 & 0 \\ 0 & 0 & 0 & 1 & L_i & 0 \\ 0 & 0 & 0 & 0 & 1 & 0 \\ 0 & 0 & 0 & 0 & 0 & 1 \end{pmatrix}, \tag{1}$$

$$T(R_i, \phi_i) = \begin{pmatrix} 1 & 0 & 0 & 0 & 0 & 0 \\ -\dfrac{2}{R_i \cos\phi_i} & 1 & 2\theta_{xi} & 0 & 0 & 0 \\ 0 & 0 & 1 & 0 & 0 & 0 \\ 0 & 0 & 0 & 1 & 0 & 0 \\ 0 & 0 & 0 & -\dfrac{2\cos\phi_i}{R_i} & 1 & 2\theta_{yi} \\ 0 & 0 & 0 & 0 & 0 & 1 \end{pmatrix}, \tag{2}$$

and

$$T(\theta_i) = \begin{pmatrix} \cos\theta_i & 0 & 0 & -\sin\theta_i & 0 & 0 \\ 0 & \cos\theta_i & 0 & 0 & -\sin\theta_i l & 0 \\ 0 & 0 & 1 & 0 & 0 & 0 \\ \sin\theta_i & 0 & 0 & \cos\theta_i & 0 & 0 \\ 0 & \sin\theta_i & 0 & 0 & \cos\theta_i & 0 \\ 0 & 0 & 0 & 0 & 0 & 1 \end{pmatrix}, \tag{3}$$

respectively, where ϕ_i is the incident angle, θ_i is the rotary angle, and θ_{xi} and θ_{yi} are the misalignment angles of mirror M_i in its local tangential and sagittal planes, respectively. Mirror tilts and length change are two types of manufacturing errors. In this letter, however, we focus on mirror tilts as the main source of optical axis variations.

The total round-trip ray matrix in a resonator is the product of each individual matrix in a proper sequential order:

$$T = \prod T_i, \tag{4}$$

where

$$T_i = T(\theta_i) \cdot T(R_i, \phi_i) \cdot T(L_i). \tag{5}$$

The optical axis is given by the eigenvector of T with an eigenvalue of 1. Therefore, the optical axis inside the crystal is an invariant in the round-trip propagation:

$$\begin{pmatrix} r_x \\ r'_x \\ 1 \\ r_y \\ r'_y \\ 1 \end{pmatrix} = T \begin{pmatrix} r_x \\ r'_x \\ 1 \\ r_y \\ r'_y \\ 1 \end{pmatrix}. \tag{6}$$

Equation (6) can be solved in a simple formulation:

$$\begin{pmatrix} T_{11}-1 & T_{12} & T_{14} & T_{15} \\ T_{21} & T_{22}-1 & T_{24} & T_{25} \\ T_{41} & T_{42} & T_{44}-1 & T_{45} \\ T_{55} & T_{52} & T_{54} & T_{55}-1 \end{pmatrix} \times \begin{pmatrix} r_x \\ r'_x \\ r_y \\ r'_y \end{pmatrix} = - \begin{pmatrix} T_{13}+T_{16} \\ T_{23}+T_{26} \\ T_{43}+T_{46} \\ T_{53}+T_{56} \end{pmatrix}, \tag{7}$$

where the optical axis decentrations r_x and r_y are the heights between the actual and ideal optical axes along the x and y axes, respectively. On the input-output coupling surface or mirror M_1, the optical axis decentration can also be represented by the distance between the actual and ideal positions of point A (i.e., the closing point of the ring cavity). The optical axis tilts r'_x and r'_y are the angles between the actual and ideal optical axes in the x and y planes, respectively. Solving Eq. (7) can derive the optical axis decentration (r_x, r_y) and tilt (r'_x, r'_y) under the influence of any misalignment of the optical components.

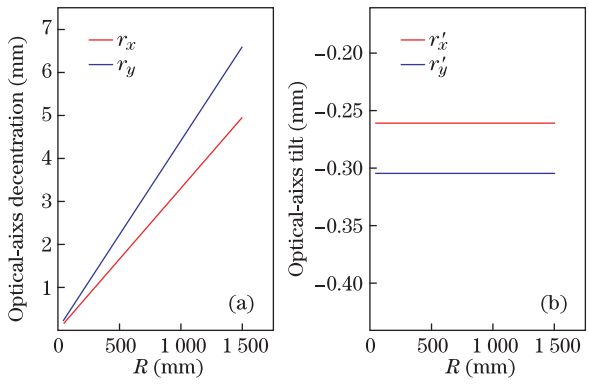

Fig. 4. (Color online) Optical axis variations as a function of R, where α=22.86°, β=45°, AE=10 mm, and CE=1.06 mm. (a) Optical axis decentration; (b) optical axis tilt.

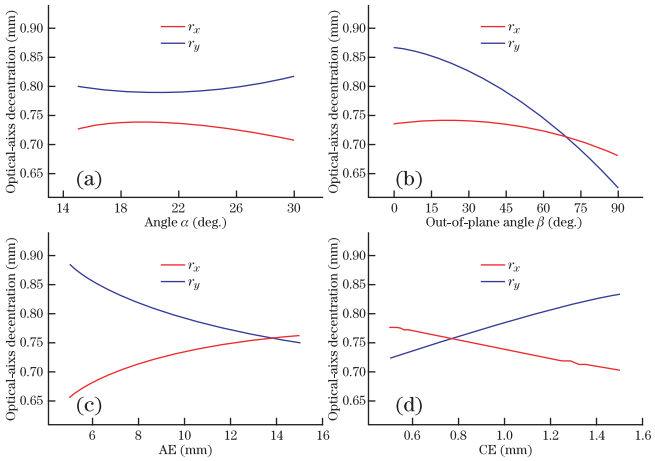

Fig. 5. (Color online) Optical-axis decentration as a function of the structure parameters, where R=200 mm. (a) AE=10 mm, CE=1.06 mm, and β=45°; (b) AE=10 mm, CE=1.06 mm, and α=22.86°; (c) CE=1.06 mm, α=22.86°, and β=45°; (d) AE=10 mm, α=22.86°, and β=45°.

In considering the end-face deformation caused by thermal effects, the self-consistence of the optical axis can be obtained with Eq. (7) under the misalignments of mirrors M_1, M_2, M_3, or M_4. Reducing the requirements in the manufacture of monolithic crystal is advantageous.

After a NPRO crystal is fabricated, errors are found on each surface and are fixed, and this means that the mirror misalignments in the four-equal-sided nonplanar ring cavity are fixed. When NPRO laser operates, the end-face deformation caused by the thermal effects varies with the pump power, and this means that the equal radius R of the mirror M_1 varies too. The relationship between the optical axis variations and the radius R of NPRO is shown in Fig. 4. The source of the optical axis variations in Fig. 4 is the tilts of mirrors M_1, M_2, M_3, or M_4 in both sagittal and tangential planes. The structure parameters of the design are α=22.86°, β=45°, AE=10 mm, and CE=1.06 mm. In the numerical analysis, each mirror tilt is assumed to be of the same value as 1 mrad. Figure 4(a) indicates that the optical axis decentration is a function of not only the manufacturing errors but also of the pump power. Moreover, the optical axis tilt is an invariant in the entire region of 50 mm $< R <$ 1500 mm, as shown in Fig. 4(b). The results demonstrate that the orientation of the laser is not determined by the pump power but by manufacturing errors only.

The analyses in this letter are based on the traditional coordinate system (TCS). Nevertheless, a novel coordinate system (NCS) was proposed by Yuan *et al.*[17–20] For comparison, we also applied the NCS and found that the results obtained from both TCS and NCS are similar to each other and lead to the same conclusion. The difference is that the optical axis tilt varies with R, as shown in Fig. 4(b). However, if R is not smaller than 300 mm, the optical axis tilt remains an approximate invariant.

A further analysis of Fig. 4(a) shows that the actual closing point A of the optical axis within the input–output coupling surface moves closer to the ideal point as R decreases. As commonly known, the radius induced by the end-face deformation decreases with an increase in pump power. Therefore, the analysis above offers a theoretical guide to the adjustment of the pump. To match the actual optical axis within the cavity, the optical axis of the pump beam must first deviate from the ideal optical axis. Then, the axis of the pump beam must be adjusted as the pump power is increased to continuously match the actual optical axis. When the pump power is fixed, the location and orientation of the pump beam should also be fixed to maximize the output power.

A good NPRO design should ensure that the optical axis variations are minimal or even near zero when the laser is operated. As such, the structure parameters of a NPRO crystal must be optimized. The optical axis variations as functions of the structure parameters α, β, AE, and CE are calculated, as shown in Figs. 5 and 6.

The optical axis decentration in the monolithic nonplanar ring resonator is shown in Figs. 5(a)-(d). Optical axis decentration varies across a wider range with parameters β, AE, and CE than with parameter α. The optical axis decentration is sensitive with parameter β. The optical axis decentration in the sagittal and tangential planes decreases as parameters α, AE, and CE increase. However, with an increase in parameter β from 0° to 90°, the optical axis decentrations in both the sagittal and tangential planes decrease.

The optical axis tilt in the monolithic nonplanar ring resonator is shown in Figs. 6(a)-(d). Interestingly, the dependence of the optical axis tilt on the parameters is similar to that of the optical-axis decentration. The optical axis tilt is sensitive with parameter β. The optical axis tilt in the sagittal and tangential planes decreases as parameters α, AE, and CE increase, but it remains constant as parameter β increases. These results demonstrate that optical axis variations should appear in any NPRO design as long as manufacturing errors exist. Because the optical-axis tilt is an invariant with the change of pump power, as shown in Fig. 4(b), a large β value reduces the influence of optical axis variations induced by the adjustment of the pump power.

In our experiment, NPRO with parameters of α=22.86°, β=45°, AE=10 mm, and CE=1.06 mm, is

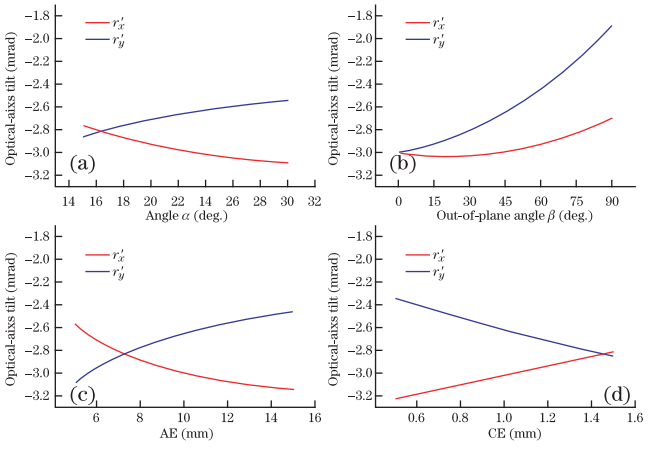

Fig. 6. (Color online) Optical axis tilt as a function of the structure parameters, where R=200 mm. (a) AE=10 mm, CE=1.06 mm, and β=45°; (b) AE=10 mm, CE=1.06 mm, and α=22.86°; (c) CE=1.06 mm, α=22.86°, and β=45°; (d) AE=10 mm, α=22.86°, and β=45°.

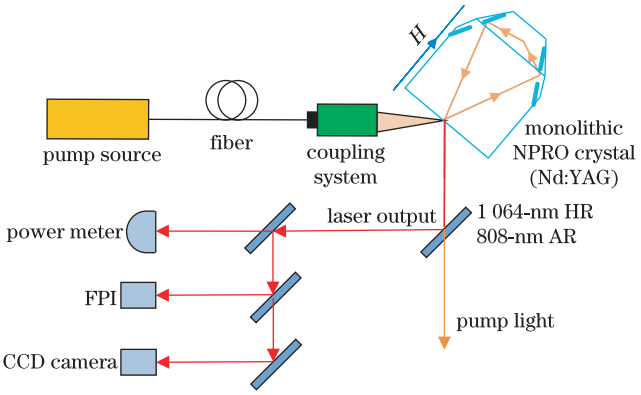

Fig. 7. (Color online) Schematic of monolithic Nd:YAG NPRO laser end-pumped by 808-nm laser diode. H: magnetic field; FPI: Fabry–Perot interferometer.

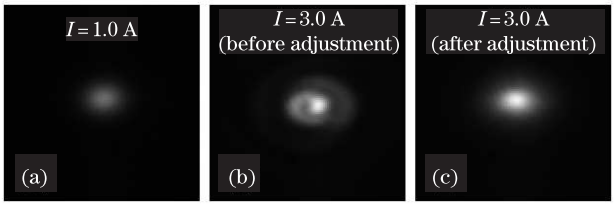

Fig. 8. Relationship between the transverse mode and the pump current. (a) I=1.0 A; (b) I=3.0 A; (c) I=3.0 A.

fabricated and used. The dimensions of the entire block are 13 (length) × 11 (width) × 3 (height) (mm). The round-trip path length of NPRO is 30.4 mm, and the optical path inside NPRO is 55.3 mm. The Nd-doping concentration is 1 at.-%. Figure 6 shows the experimental setup of monolithic Nd:YAG NPRO pumped by an 808-nm fiber-coupled laser diode with an emitting aperture of 105 μm and a numerical aperture of 0.22. The pump beam was collimated and focused into Nd:YAG NPRO by a 1:1 coupling optical system. A permanent magnetic field of 0.2 T in the direction shown in Fig. 7 was applied to obtain unidirectional oscillation. The input–output coupling surface was coated for a high transmission at 808 nm and for a 3.0% transmittivity of the s-polarized beam at 1064 nm. A thermal electric cooler was used to control the temperature of Nd:YAG NPRO.

The minimal value of the NPRO laser threshold was obtained at 0.19 W by adjustment of the axis of the pump beam. The laser output power linearly increased with the pump power. The optical axis decentration caused by the increase in the pump power is so small that the specific value of the optical axis decentration cannot be directly obtained with a charge-coupled device (CCD) camera. When optical axis decentration occurs, the overlap between the pump beam and the oscillating beam becomes small, a phenomenon called off-axis pumping. As described in Ref. [21], high-order transverse modes can be generated through the method of off-axis pumping. Therefore, optical axis decentration can be verified from the generation of high-order transverse modes caused by off-axis pumping. The transverse modes of the output beam were monitored by a CCD camera. Figure 8 shows the typical shift of the transverse modes with an increase in the pump power. The transverse mode is the fundamental mode when the incident pump current is 1.0 A, as shown in Fig. 8(a). When the pump current is increased to 3.0 A, high-order transverse modes are observed, as shown in Fig. 8(b), and this means that off-axis pump occurs. With the pump position finely adjusted, the transverse mode of the output beam returns to the fundamental mode, as shown in Fig. 8(c). The position of the laser spot center does not significantly change in Figs. 8(a) and (c), and this result confirms that the optical axis tilt remains constant as the pumping power increases.

The output power monitored by a power meter increases after the pump position is adjusted, as shown in Fig. 9. The output power of Nd:YAG NPRO laser after adjustment is 1.06 W when the pump current is 3.0 A. It increases by 6.0% relative to the output power of 1.00 W before adjustment. Figure. 8 shows that the obtained maximum value of the single-frequency output power is 1.32 W, and the corresponding optical-optical efficiency is 51.2%. The experimental results demonstrate the existence of optical axis decentration and verify the expectation on the pump beam adjustment of our mathematical model. Therefore, a theoretical basis is provided to further optimize NPRO laser.

The single-longitudinal-mode spectrum was monitored by a scanning confocal Fabry–Perot interferometer (FPI) with a free spectral range of 1.5 GHz. The output signals from the FPI at the maximum output power indicate that NPRO laser was in single-frequency operation.

In conclusion, the optical axis variations in monolithic nonplanar ring laser are theoretically and experimentally investigated. The results show that the self-consistence of the optical axis can always be obtained because of thermal effects. For the nonplanar ring resonator with a fabricated crystal, optical axis variations appear in any NPRO design as long as manufacturing errors exist. The location of the closing point A within the input–output coupling surface varies with the mirror misalignments and curvature radius induced by thermal effects. The actual location of point A on the optical axis moves close to the ideal point as the pump power increases. The optical axis tilt remains an invariant with any changes in the pump power. A large value of the structure parameter β results in a stable optical axis laser. The experimental results verify the theoretical analysis. The single-frequency output power after adjustment increases by 6.0% relative to the output power before adjustment.

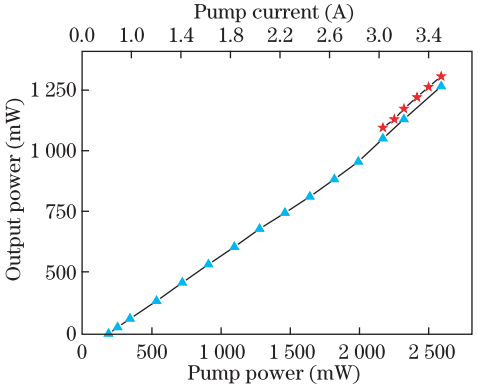

Fig. 9. (Color online) Output power versus pump power.

This work was supported by the Chinese and Israeli Cooperation Project on High Power Laser Technology under Grant No. 2010DFB70490.

References

1. T. J. Kane and R. L. Byer, Opt. Lett. **10,** 65 (1985).
2. T. J. Kane, A. C. Nilsson, and R. L. Byer, Opt. Lett. **12,** 175 (1987).
3. I. Freitag, A. Tünnermann, and H. Welling, Opt. Commun. **115,** 511 (1995).
4. J. Yang, Y. Tang, and J. Xu, Photon. Res. **1,** 52 (2013).
5. T. J. Kane, W. J. Kozlovsky, and R. L. Byer, Opt. Lett. **12,** 239 (1987).
6. Y. Zheng, C. Gao, R. Wang, M. Gao, and Q. Ye, Opt. Lett. **38,** 784 (2013).
7. C. Gao, M. Gao, Y. Zhang, Z. Lin, and L. Zhu, Opt. Lett. **34,** 3029 (2009).
8. M. Gao, Y. Zhao, L. Zhang, L. Wang, and C. Gao, Chin. Opt. Lett. **11,** 041406 (2013).
9. A. C. Nilsson, E. K. Gustafson, and R. L. Byer, IEEE J. Quantum Electron. **25,** 767 (1989).
10. E. Zang, J. Cao, M. Zhong, C. Li, N. Shen, D. Hong, L. Cui, Z. Zhu, and A. Liu, Appl. Opt. **41,** 7012 (2002).
11. J. Xu, J. Zhu, and F. Liu, Chin. Opt. Lett. **10,** 091401 (2012).
12. F. Liu, Z. Liu, L. Zheng, H. Huang, and J. Zhu, High Power Laser Sci. Eng. **1,** 29 (2013).
13. J. Yuan and X. Long, Opt. Commun. **281,** 1204 (2008).
14. S. -C. Sheng, Opt. Lett. **19,** 683 (1994).
15. A. E. Siegman, in *Lasers* A. Kelly, (ed.) (University Science Books, 1986) pp. 581-624.
16. A. H. Paxton and W. P. Latham Jr., Appl. Opt. **25,** 2939 (1986).
17. J. Yuan, M. Chen, Z. Kang, and X. Long, Opt. Lett. **37,** 2082 (2012).
18. J. Yuan, M. Chen, Z. Kang, and X. Long, Opt. Express **21,** 2297 (2013).
19. M. Chen, J. Yuan, X. Long, Z. Kang, and Y. Li, Optik **124,** 6776 (2013).
20. J. Yuan, X. Long, and L. Liang, Appl. Opt. **46,** 6314 (2007).
21. Y. F. Chen, T. M. Huang, C. L. Wang, and S. C. Wang, IEEE J. Quantum Electron. **33,** 1025 (1997).